Biochemical Journal (2021) **478** 1333–1346
https://doi.org/10.1042/BCJ20210021

Research Article

Excitation energy transfer kinetics of trimeric, monomeric and subunit-depleted Photosystem I from Synechocystis PCC 6803

Parveen Akhtar[1], Avratanu Biswas[1,2], László Kovács[1], Nathan Nelson[3] and Petar H. Lambrev[1]

[1]Biological Research Centre, University of Szeged, Temesvári krt. 62, Szeged 6726, Hungary; [2]Doctoral School of Biology, University of Szeged, Közép Fasor 52, Szeged 6726, Hungary; [3]Department of Biochemistry and Molecular Biology, The George S. Wise Faculty of Life Sciences, Tel Aviv University, Tel Aviv 69978, Israel

Correspondence: Petar H. Lambrev (lambrev.petar@brc.hu)

Photosystem I is the most efficient photosynthetic enzyme with structure and composition highly conserved among all oxygenic phototrophs. Cyanobacterial Photosystem I is typically associated into trimers for reasons that are still debated. Almost universally, Photosystem I contains a number of long-wavelength-absorbing 'red' chlorophylls (Chls), that have a sizeable effect on the excitation energy transfer and trapping. Here we present spectroscopic comparison of trimeric Photosystem I from *Synechocystis* PCC 6803 with a monomeric complex from the Δ*psaL* mutant and a 'minimal' monomeric complex ΔFIJL, containing only subunits A, B, C, D, E, K and M. The quantum yield of photochemistry at room temperature was the same in all complexes, demonstrating the functional robustness of this photosystem. The monomeric complexes had a reduced far-red absorption and emission equivalent to the loss of 1.5–2 red Chls emitting at 710–715 nm, whereas the longest-wavelength emission at 722 nm was not affected. The picosecond fluorescence kinetics at 77 K showed spectrally and kinetically distinct red Chls in all complexes and equilibration times of up to 50 ps. We found that the red Chls are not irreversible traps at 77 K but can still transfer excitations to the reaction centre, especially in the trimeric complexes. Structure-based Förster energy transfer calculations support the assignment of the lowest-energy state to the Chl pair B37/B38 and the trimer-specific red Chl emission to Chls A32/B7 located at the monomer–monomer interface. These intermediate-energy red Chls facilitate energy migration from the lowest-energy states to the reaction centre.

Introduction

Photosystem I (PSI) is a membrane-bound pigment-protein complex essential for all oxygen-evolving photosynthetic organisms. It has a highly conserved structure and composition [1–3]. PSI consists of 11–14 protein subunits coordinating 94–96 chlorophylls (Chls), ∼24 carotenoids (Cars) and other cofactors [4–6]. In cyanobacteria, PSI is usually found in a trimeric or monomeric form, though recently, tetrameric forms have been reported in heterocyst-forming species [7]. The oligomerization state may change towards the monomeric form under different growth conditions, such as light, temperature and available nutrients [8–10]. In PSI of the model cyanobacterium *Synechocystis* PCC6803, 86 Chls are associated with the two largest central subunits of the heterodimeric core, PsaA and PsaB, while 9 Chls are bound to the smaller subunits F, J, K, L, and M [6,11]. PsaL, a 16 kDa hydrophobic protein subunit of the PSI core, was found to be essential for the formation of trimers [12]. The rest of the small subunits, however, could each be deleted without observing any severe growth defects in cells [12,13]. A minimal PSI complex from *Synechocystis*, consisting only of A, B, C, D, E, K and M subunits, has been recently obtained and crystalized; however, no high-resolution structure could be resolved, casting some doubt on the intactness of the complex [6].

Received: 11 January 2021
Revised: 3 March 2021
Accepted: 9 March 2021

Accepted Manuscript online: 9 March 2021
Version of Record published: 6 April 2021

Biochemical Journal (2021) 478 1333–1346
https://doi.org/10.1042/BCJ20210021

PSI of almost all organisms contains long-wavelength Chl forms, dubbed 'red' Chls, absorbing light at wavelengths longer than the absorption of the reaction centre (RC) Chls P_{700} [14,15], and thus broadening the absorption spectral range. The red Chls have unusual spectroscopic properties, such as large bandwidth, Stokes shift and electron-phonon coupling, that result from the mixing of excitonic and charge-transfer (CT) states [16,17]. The number of red Chls and their spectral properties vary among species and oligomeric forms of PSI. Deconvolution analyses of the absorption spectra of PSI of *Synechocystis* PCC 6803 [18] and spectral hole-burning studies [19,20] have indicated that ∼5 red Chls are present in trimers and ∼3 in monomers. It has been recognized that the red forms originate from strong Coulombic interactions between the Chls and several candidate pigments (or pigment groups) have been proposed [4,21–26], but these assignments remain largely hypothetical.

Although the red Chls account for only a small fraction of the total absorption cross-section [27], they have sizeable impact on the dynamics of energy transfer (ET) and trapping, as the ET from the red Chls to the RC is energetically uphill and thermally activated [28,29]. At cryogenic temperatures, the thermal energy is not sufficient for the uphill ET and the long-wavelength pigments act as (pseudo)traps increasing the excited-state lifetime in this region and dominating the fluorescence emission [28,30]. Energy equilibration between the bulk antenna Chls and the low-energy pigments absorbing below 700 nm is shown to take 2–4 ps in PSI from *Synechocystis* sp. PCC 6803 at room temperature (RT) [18,31–35] – significantly faster than the effective photochemical trapping time of ∼20 ps. Recently, significantly slower lifetimes of ET have been uncovered in the PSI core from higher plants at a cryogenic temperature [36]. Very few low-temperature time-resolved fluorescence studies have been reported for cyanobacterial PSI and only for thermophilic species, containing a greater number of red Chls [37,38].

Because of its high quantum efficiency, relative abundance and structural and functional stability, cyanobacterial PSI is an attractive candidate for the development of bio-hybrid devices for solar energy conversion and biosensor applications [39–41]. Engineering a 'minimal' PSI with reduced protein content, requiring less cellular resources to produce and a smaller footprint but retaining full functionality can evidently be advantageous for such developments. Here we report a comparative investigation of PSI trimers and monomers from *Synechocystis* PCC 6803 as well as subunit-depleted 'minimal' PSI ΔFIJL with a focus on the pigment spectral forms affected by the oligomerization state and subunit depletion and on the excitation dynamics at room and low temperature. Previously, it has been shown that monomers exhibit differences in absorption, emission, and circular dichroism (CD) spectra compared with trimers [10,42]. We examined these difference in detail to determine the pigment groups and interactions underlaying them. While trimers and monomers showed similar trapping times at RT [18,32], specific differences are observed in the kinetics of equilibration with the red Chls at 77 K. We confirm that the subunit-depleted PSI is fully functional with indistinguishable picosecond excitation kinetics.

Materials and methods

Cell culture

Cyanobacterial cells were grown in BG11 medium supplemented with 5 mM HEPES–NaOH (pH 7.5). *Synechocystis* sp. PCC 6803 wild-type (WT), Δ*psaL* [10] and the ΔFIJL [6] strains were grown photoautotrophically on a rotary shaker (100 rpm) at 30°C under continuous white light (∼35 μmol photons m^{-2} s^{-1}). The minimal PSI was obtained from a strain constructed from the ΔFIJL mutant, deleting the PsaJ-PsaF operon, described elsewhere [6]. For the Δ*psaL* cells, the medium was supplemented with 40 μg/ml spectinomycin and for PSI minimal with 10 μg/ml kanamycin, and 6 μg/ml chloramphenicol.

Thylakoid membranes preparation

Thylakoid membranes were isolated following the protocol of Zakar et al. [43]. One-week old cells were harvested and washed in buffer A (20 mM MES/NaOH, pH 6.4, 10 mM $MgCl_2$, 10 mM $CaCl_2$) at RT by centrifugation for 5 min at 6000***g***. The pelleted cells were resuspended in buffer A supplemented with 25% glycerol, 0.5 mM phenylmethanesulfonyl fluoride and 1 mM benzamidine and broken with glass beads (≤106 μm) using a Mini bead beater (Precellys Evolution) equipped with a dry ice cooling compartment. After breaking, the suspension was centrifuged (4°C, 6 min, 4000***g***) to remove the cell debris and remaining glass beads. Then the supernatant was further centrifuged for 30 min at 30 000***g***, 4°C and the pellet was solubilized in buffer A and used for further experiments.

Photosystem I preparation

PSI samples were isolated from freshly prepared thylakoid membranes following the protocol of Vajravel et al. [42]. The thylakoid membranes were solubilized by incubating with 2% n-dodecyl β-D-maltoside (β-DDM) at 4°C for 30 min. The suspension was centrifuged for 15 min at 10 000***g*** to remove the unsolubilized material. The supernatant was then loaded on a stepwise (6 steps, 0.2–0.9 M) sucrose gradient containing 20 mM HEPES (pH 7) and 0.05% of β-DM followed by centrifugation at 220 000***g*** for 17–18 h at 4°C. The gradient fractions containing PSI trimers (from WT) and monomers (from WT, Δ*psaL* and ΔFIJL mutant) were collected by a syringe. The samples were washed in a medium containing 0.03% β-DDM, concentrated using Amicon Ultra filters (Millipore) and stored at −80°C until use.

Additional experiments were performed on PSI minimal suspension obtained by incubating the crystals [6] in a buffer medium containing 0.03% β-DDM (while agitating).

Pigment analysis

The pigment composition of all samples (thylakoid membranes, purified complexes) was determined by fitting the acetone extract spectra in the visible range from 350 to 750 nm with the spectra of the individual pigments. Absorption spectra of pure Chl *a* (Sigma–Aldrich) and Cars extracted from the thylakoid membranes were recorded in 80% acetone. Then these spectra were used as a reference to obtain a fit of the spectra of the acetone extracts of PSI samples. Molar absorption coefficients were taken from Lichtenthaler [44]. For analysis of the Chls and Cars composition by high-performance liquid chromatography, the pigments were extracted in pure acetone and the quantification was performed using a Shimadzu Prominence HPLC system as described in Zsiros et al. [45]. The pigments were identified according to their retention time and absorption spectrum and quantified by integrated chromatographic peak area recorded at the wavelength of maximum absorbance for each kind of pigments using the corresponding molar decadic absorption coefficient [46].

Absorption and circular dichroism spectroscopy

Absorption and circular dichroism spectra in the range of 350–750 nm were recorded at RT with a Thermo Evolution 500 dual-beam spectrophotometer and a Jasco J-815 spectropolarimeter, respectively. The samples were diluted in 20 mM Tricine buffer (pH 7.5) with 0.03% β-DDM to an absorbance of one at the red maximum. The measurements were performed in a standard glass cell of 1 cm optical path length with 1 nm (absorption) or 2 nm (CD) spectral bandwidth.

Time-resolved fluorescence

Fluorescence decays were recorded by time-correlated single-photon counting (TCSPC) using an instrument described in Akhtar et al. [47] at emission wavelengths 664–744 nm with 8 nm steps, at RT, and 670–750 nm with 5 nm steps at 77 K. The source of excitation was a Fianium WhiteLase Micro (NKT Photonics, U.K.) supercontinuum laser, providing pulses at a repetition rate of 20 MHz centred at 440 nm. The total instrument response (IRF) width was 40 ps, measured using 1% Ludox as scattering solution. The samples were diluted to an absorbance of 0.05 (1 mm optical path length) at the excitation wavelength in buffer medium containing 50% (v/v) glycerol, 20 mM tricine and 0.03% β-DDM. The suspension was cooled to 77 K in an optical cryostat (Optistat DN, Oxford Instruments, U.K.). For measurements with closed (oxidized) RCs, 1 mM potassium ferricyanide was added and the sample was preilluminated with white light for 5 min before freezing in liquid nitrogen. Control experiments were performed with dark-adapted samples frozen in the presence of 40 μm phenazine methosulfate and 40 mM sodium ascorbate and attenuating the excitation intensity 20-fold.

Structure-based modelling of the excitation dynamics

Semi-quantitative calculations of the dynamics of ET in PSI were performed using Förster theory as described in Byrdin et al. [23] with the assumptions and limitations therein and with modifications as follows. Distances, relative orientations and electronic couplings between Chls are calculated using atomic coordinates in the trimeric PSI structure of *Synechocystis* PCC 6803 [6]. Excitonic interactions are neglected, except for the RC Chls. All bulk Chls are assigned gaussian absorption lineshapes with central wavelengths normally distributed within the Q_y absorption band and uniform widths ($\sigma = 80\ cm^{-1}$) along with two vibronic/Q_x sidebands shifted by 1100 and 2300 cm^{-1}. The fluorescence spectra mirror the absorption spectra with a Stokes shift of 140 cm^{-1}. Separate spectral parameters are set for the RC and linker Chls as well as for the designated red Chls. The

Biochemical Journal (2021) **478** 1333–1346
https://doi.org/10.1042/BCJ20210021

absorption/emission spectra are calculated for 1000 random realizations and Förster ET rates are estimated for each Chl pair based on the distance, orientation and spectral overlap. Additional decay rates of 0.5 ns^{-1} and 1 ps^{-1} are imposed for all antenna Chls and for P_{700}, respectively. The population kinetics is calculated by inverting the transfer rate matrix. Fluorescence decays at different wavelengths are calculated from the time-dependent population and the fluorescence emission spectra. Simulated fluorescence data are generated by convolving the disorder-averaged decays with a model IRF and adding Poisson noise.

Results

Absorption and CD spectra

The absorption spectra of trimeric and monomeric PSI complexes isolated from *Synechocystis* WT, Δ*psaL* and ΔFIJL are compared in Figure 1. Both types of monomeric PSI show significantly lower absorption at wavelengths longer than 690 nm in line with numerous studies that have reported loss of red-shifted Chl forms upon monomerization. The absorption difference spectra show a positive peak ∼ 692–696 nm and a negative peak at 676–677 nm. The magnitude of the differences approximately corresponds to the missing antenna Chls (3 in Δ*psaL* and 7 in ΔFIJL). The difference absorption band at 620 nm is due to a small phycocyanin contamination in the monomeric preparations. The ratio of the integrated absorption spectrum beyond 700 nm to the total area under the main Q_y absorption band (650–720 nm) corresponds to ∼3.5 'red Chls' in both monomeric PSI types and five in the trimeric PSI (Supplementary Table S1), in agreement with previous studies [18].

The L subunit of PSI binds two Cars and the F, I and J subunits bind five more [5,6]. Accordingly, the monomeric PSI complexes, especially ΔFIJL, have decreased absorption ∼ 500 nm. The HPLC analysis showed 15–30% lower content of carotenes, echinenone and zeaxanthin in the ΔFIJL PSI (Supplementary Figure S1, Supplementary Table S2). For a more precise quantification we performed spectral decomposition of the absorption spectra of acetone pigment extracts from the three PSI types using purified Chl *a* and total Cars extracted from the thylakoid membranes (Supplementary Figure S2). From the fits we estimate 24, 22 and 17 Cars in PSI from WT, Δ*psaL* and ΔFIJL, respectively. The values exactly match the expected number of Cars, confirming that no additional pigments or subunits were lost during the isolation of PSI.

CD spectra were recorded to test for possible changes in the pigment exciton interactions (Figure 2). In the red region, the amplitude of the negative excitonic CD band (688 nm) diminished by 25% in both monomeric PSI types with no distinguishable difference among the two. In the blue-green region, the CD spectrum of PSI WT shows an intense broad band with a maximum at 505 nm, originating mainly from β-carotenes. It was previously observed that this band is sensitive to the oligomerization of PSI [10,42] and can be used as a fingerprint of trimeric PSI *in vivo* as well as in isolated complexes [48]. The band intensity was 58% smaller in Δ*psaL* complexes relative to WT PSI, whereas the absorption in this region is hardly affected (as Δ*psaL* PSI contains just two Cars less than WT). The exact same result was obtained from monomers isolated from WT

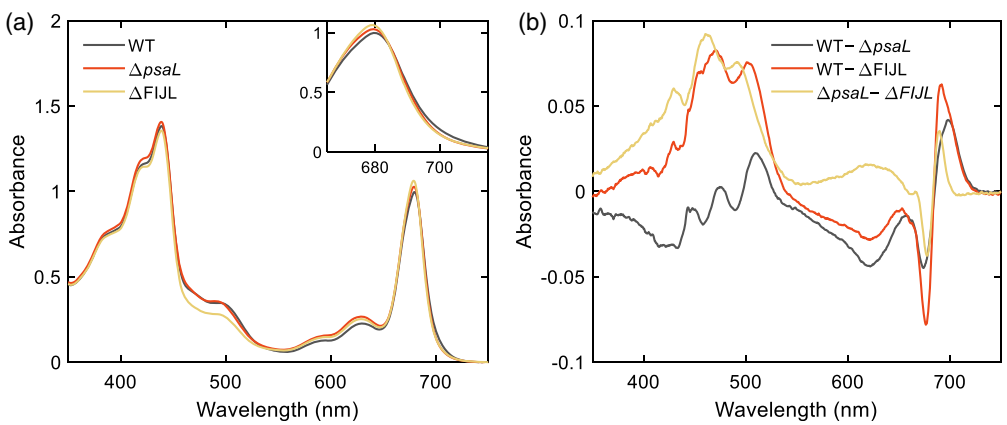

Figure 1. Absorption spectra of isolated PSI complexes from *Synechocystis* WT, Δ*psaL* and ΔFIJL.

(**a**) Average spectra from four independent preparations, normalized to the area between 650 and 720 nm. (**b**) Absorption difference spectra.

Biochemical Journal (2021) **478** 1333–1346
https://doi.org/10.1042/BCJ20210021

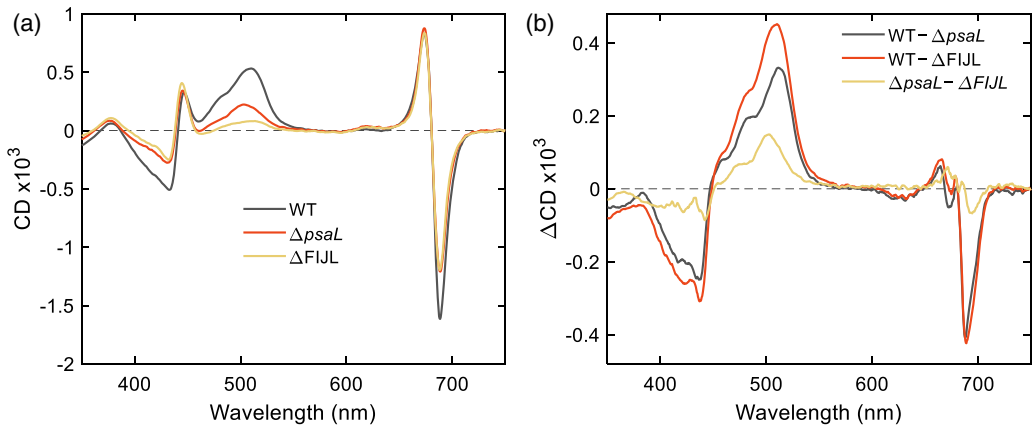

Figure 2. CD spectra of isolated PSI complexes from *Synechocystis* WT, *ΔpsaL* and ΔFIJL.
(**a**) Average spectra normalized to unity absorption at the red maximum. (**b**) CD difference spectra.

cells as well (Supplementary Figure S3). Even more striking is the 85% loss of CD_{505} in the minimal PSI, where the total Car content is reduced by 29% (Supplementary Figure S2). Virtually identical CD spectra were recorded from the thylakoid membranes of WT, Δ*psaL* and ΔFIJL (Supplementary Figure S4) — ruling out the possibility that the differences are due to the PSI isolation procedure.

Fluorescence kinetics at RT

The RT fluorescence decay curves over a 2 ns time period were subjected to global analysis with a three-exponential model. The main fluorescence decay lifetime (with 98% amplitude) of trimeric PSI isolated from WT *Synechocystis* was 25 ± 1 ps (Table 1) — this is the effective trapping time of antenna excitations [31,34,49]. No differences in the trapping time were detected in the monomeric PSI types. The other two long-lived components are from contaminations from uncoupled Chls and Photosystem II (PSII). Hence, the decay-associated spectrum (DAES) of the 25 ps component (Figure 3) is equivalent to the (stationary) emission spectrum of the pure PSI. The spectra of the monomeric PSI clearly show lower amplitudes at 700–720 nm compared with the trimeric one. Virtually identical PSI spectra (and lifetimes) were recorded from monomeric PSI isolated from WT cells (Supplementary Figure S5) as well as from thylakoid membranes and whole cells — confirming that the differences are relevant *in vivo* (Supplementary Figure S6).

The RT emission spectrum of PSI represents a thermal quasiequilibrium between all emitting Chls — bulk and red — and can reveal the different red spectral forms and their abundance. Note that the steady-state emission spectrum measured from trimeric and monomeric PSI [32], is not suitable for such quantification because of the very high relative fluorescence yield of the free Chls and PSII. We decomposed the 25 ps DAES into two 'bulk' Chl pools and three red pools emitting at 707, 715 and 720 nm (see Supplementary Table S3 and accompanying text on the details of the calculation). A near-perfect fit of the trimeric PSI spectrum (Figure 3) was obtained with 89 bulk Chls plus 4 emitting at 707 nm and one at 715–720 nm. The best fit for both monomeric PSI types was achieved by decreasing the 707 nm pool by ∼2 Chls. Thus, the quantification of the red states from the DAES is in agreement with the analysis of the absorption spectra, while additionally revealing the emitting wavelength of the red Chls lost in monomers.

Table 1 Fluorescence decay lifetimes and amplitudes of PSI complexes at RT

	τ_1 (ps)	a_1 (%)	τ_2 (ps)	a_2 (%)	τ_3 (ns)	a_3 (%)
WT	25 ± 1.1	98.4	246 ± 20	0.4	4.1 ± 0.5	1.2
Δ*psaL*	24 ± 0.4	93.7	248 ± 20	3.1	3.1 ± 0.1	3.2
ΔFIJL	24 ± 0.4	94.4	241 ± 12	2.5	3.2 ± 0.2	3.1

Biochemical Journal (2021) **478** 1333–1346
https://doi.org/10.1042/BCJ20210021

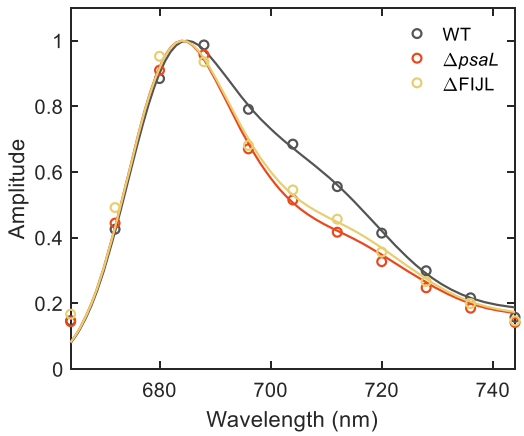

Figure 3. Decay-associated emission spectra obtained from global analysis of the fluorescence decays of PSI recorded at RT.

The spectra correspond to the decay components with lifetimes of 24–25 ps. The solid lines represent simulated spectra as described in the text. Long-lived components with very small amplitudes are not plotted.

Fluorescence kinetics at 77 K

Time-resolved fluorescence measurements were performed at 77 K to resolve the dynamics of excitation relaxation and trapping by the different pools of red Chls. Six lifetimes were necessary to fit the fluorescence decays at 670–750 nm over a 4 ns time period. As excitations are gradually transferred from shorter- to longer-wavelength pigments at cryogenic temperature, the DAES shift to the red (Figure 4). The two fastest components — 13–15 ps and 37–44 ps — show transfer from 690 nm to 700–710 nm and from 700 nm to 715–725 nm. The long-lived components with lifetimes 130–160 ps, 410–460 ps and 1.1–1.3 ns have all-positive DAES with maxima ∼ 710, 716, and 722 nm, respectively (red-shifted by 1–2 nm in trimeric PSI). Although the lifetimes and DAES are very similar in all PSI types, some specific differences can be noted for the monomeric compared with trimeric PSI: (1) all but the first decay lifetimes are 10–25% longer; (2) the amplitudes of the DAES peaking at 710 and 715 nm are smaller — the former especially is reduced by 50%; (3) correspondingly, the negative amplitudes of the ET components at 710–716 nm are also smaller. No meaningful differences in the fluorescence kinetics or spectra were detected between the two monomeric PSI types, Δ*psaL* and ΔFIJL. Virtually the same DAES were resolved in thylakoid membranes (Figure 4d–f), apart from changes in the short-lived components below 700 nm, which evidently show PSII emission. In thylakoid membranes with monomeric PSI, the amplitude of the DAES peaking at 710 nm is reduced by half.

The changes in the fluorescence kinetics described above affect the overall excitation trapping time. The average fluorescence lifetime plotted as a function of the wavelength shows significant changes between trimeric and monomeric PSI (Figure 5). The average lifetime at 730 nm was 40% longer in *ΔpsaL* and ΔFIJL PSI compared with WT.

To test how the oxidation state of the RC may affect the fluorescence decay kinetics, measurements were also performed with P_{700} pre-oxidized by preillumination in the presence of 1 mM potassium ferricyanide. Under these conditions the average fluorescence lifetime in the far-red region was longer, mainly due to the increased relative amplitude of the 1 ns decay component. Conversely, in samples that were frozen in darkness with electron donors (ascorbate and phenazine methosulfate) to increase the proportion of open RCs, the average lifetimes at 730 nm were shorter (Table 2). These results indicate that excitations at the longest wavelength Chls can be transferred to P_{700} and used for photochemistry at 77 K.

Discussion

Induced CD of carotenoids

Of the 24 carotenoids per monomer in the trimeric PSI [6], only 20 were resolved in the monomeric $PsaL^{His}$ PSI [11] — two are missing from the L subunit and two in subunit A may be unresolved in the lower-resolution structure. Five more Cars are coordinated by the F, I, and J subunits and therefore a total of at least

Biochemical Journal (2021) **478** 1333–1346
https://doi.org/10.1042/BCJ20210021

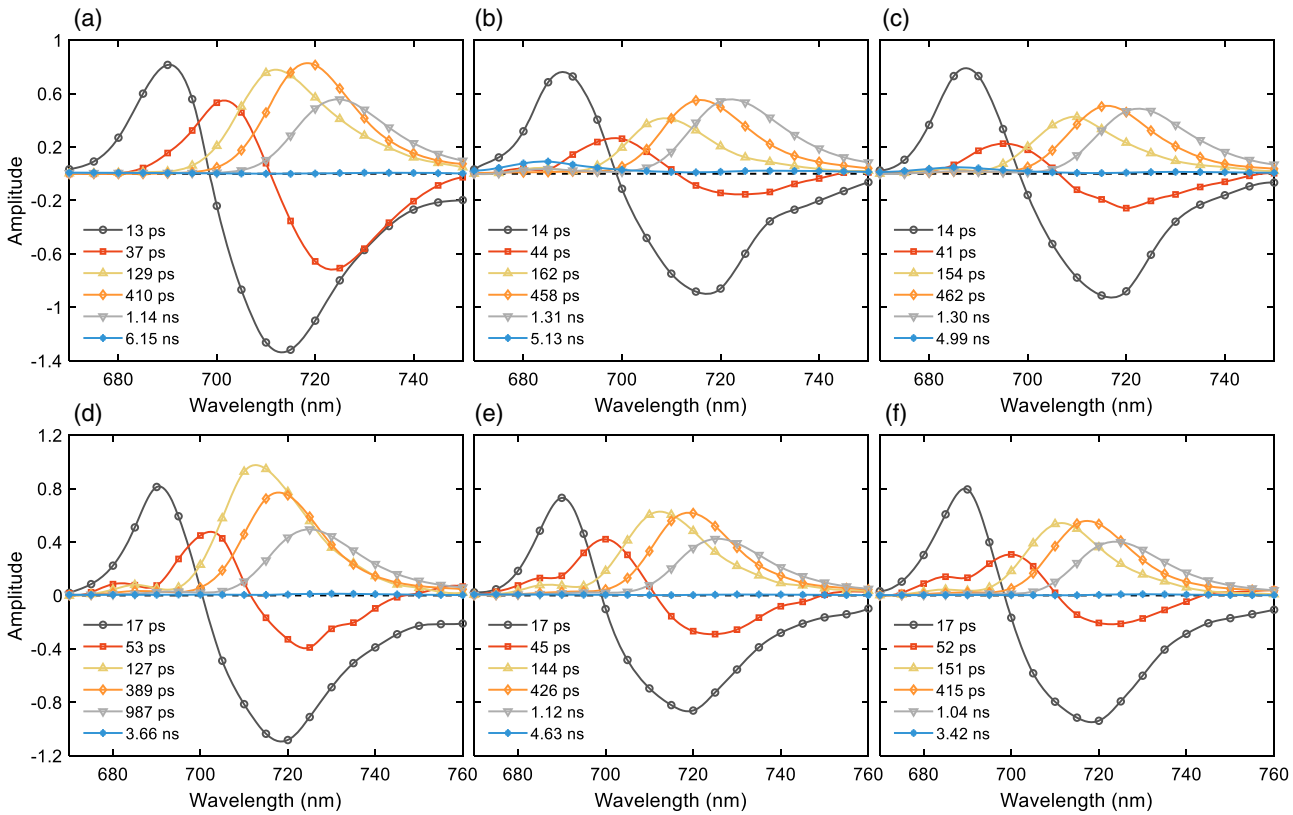

Figure 4. Decay-associated fluorescence emission spectra of isolated PSI complexes and thylakoid membranes.
(**a**–**c**) PSI complexes. (**d**–**f**) thylakoid membranes. (**a**,**c**) WT; (**b**,**e**) ΔpsaL; (**c**,**f**) ΔFIJL. The spectra are obtained from global lifetime analysis of fluorescence decays measured by TCSPC at 77 K.

seven Cars should be absent from the minimal PSI. In principle, several other Cars located between these and the 'core' subunits, could also be lost — for instance, hydroxyechinenone I4021 — but this does not seem to be the case if we rely on the quantification of pigment acetone extracts. It is remarkable then, that the loss of seven Cars results in >80% reduction in the CD intensity at 505 nm. Clearly, only a few Cars are responsible for the CD.

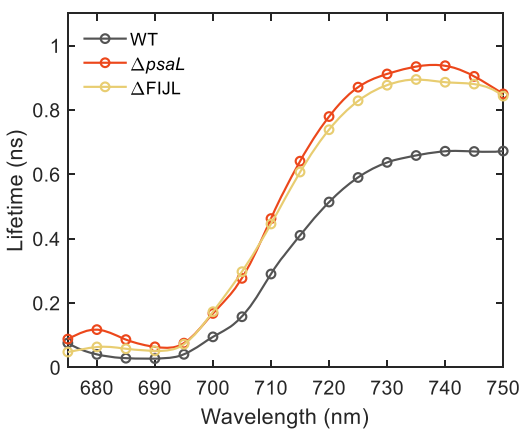

Figure 5. Wavelength dependence of the amplitude-weighted average fluorescence lifetime $\tau_{av} = \Sigma_i a_i \tau_i / \Sigma_i a_i$ for the PSI complexes at 77 K.

Biochemical Journal (2021) **478** 1333–1346
https://doi.org/10.1042/BCJ20210021

Table 2 Fluorescence decay lifetimes and average lifetime at 730 nm of PSI with preoxidized and mixed reduced/oxidized RC

	τ_3 (ps)	a_3 (%)	τ_4 (ps)	a_4 (%)	τ_5 (ns)	a_5 (%)	$\tau_{730\,nm}$ (ns)
WT (red/ox)	112	33	377	38	0.95	28	0.45
WT (oxidized)	139	29	402	34	1.10	37	0.58
ΔFIJL (red/ox)	110	19	409	28	1.01	45	0.61
ΔFIJL (oxidized)	151	18	430	30	1.30	50	0.82

Cars in solution rarely exhibit optical activity but they can acquire CD when bound to proteins [50,51]. There are two types of induced CD — one is when the achiral molecules adopt different conformations such that atom displacement breaks the molecular symmetry, and another is when the chromophores are engaged in dipole–dipole interactions creating excitonic CD. The CD difference spectra of PSI (Figure 2) suggest the former type, i.e. the Car signals are induced Cotton effects resulting from the protein environment forcing the Car molecules into a chiral conformation, rather than intermolecular excitonic interactions. Some Cars, including xanthophylls, are chiral and can have Cotton effect depending on the configuration of the polyene chain and the end cyclohexene rings. Upon crude inspection of the 24 Cars in the PSI structure, several stand out as having highly distorted polyene chains and twisted rings (Supplementary Figure S7). Interestingly, the majority of them are xanthophylls (B4011, F4016, I4020, M4021), such as zeaxanthin and echinenone, but also several carotenes and 9-cis carotenes (A4019, B4018). Despite a very minor loss of Cars in Δ*psaL* PSI (only 2–3 Cars), it has a greatly reduced CD spectrum. The CD difference spectrum shows that the missing Car is red-shifted (512 nm maximum), which may indicate a contribution from xanthophylls like echinenone that have more conjugated π-bonds compared with carotene [52]. The I subunit, shown to be lost in other psaL-deficient monomers [6], binds echinenone or other xanthophylls at position I4020 — this Car might contribute to the CD band at 511 nm. The F/J subunits bind only three Cars, including the 9-cis zeaxanthin F4016, that contribute 30% of the total CD. A more comprehensive analysis comparing PSI from different cyanobacterial strains augmented with structure-based calculations [53] could validate the assignment of the Car CD.

Red Chls in trimeric PSI

Trimeric PSI from different cyanobacterial species has been shown to contain additional red absorption that is not observed in monomers [18,20]. Upon comparison of the absorption as well as emission spectra of trimeric and monomeric PSI from *Synechocystis*, we determined that trimers contain an equivalent of 1.5–2 additional red Chls (based on equal oscillator strength). These red Chls emit with a maximum at 707–708 nm at RT (Figure 3) and 710–715 nm at 77 K (Figure 4) — in contrast, the lowest-energy states peak at 722–724 nm. Since a high-resolution crystal structure of PSI from a thermophilic cyanobacterium has been available, several groups have attempted to identify the Chls responsible for the red absorption/emission, assuming that they need to be strongly excitonically coupled [4,21,23,26]. One strongly coupled pair that has been promoted as a likely candidate for the lowest-energy red Chls is A32/B7, located at the monomer–monomer interface, close to the I/L subunits. As our time-resolved fluorescence shows, the longest-wavelength emission is hardly affected in monomeric PSI. Hence, if Chls A32/B7 give rise to the trimer-specific red absorption, they cannot harbour the lowest-energy state, as previously suggested [21,23]. We propose that A32/B7 forms a state emitting ∼ 710 nm in the trimer but is blue-shifted in the monomeric complex due its altered environment (that can modify the pigment excitonic coupling as well as the charge-transfer character of the excited state). The lowest-energy states emitting at 722–724 nm remain to be located on one or more Chls outside the monomerization region, e.g. A38/A39, B31/B32, B37/B38 [23–25,54].

Excitation dynamics in PSI

The deletion of the four subunits F, I, J, L from PSI results in discernible changes in its spectroscopic characteristics but the overall excitation trapping rate is unaffected — it remains ∼ 25 ps at RT in PSI with open RC (where we have used external electron donors to quickly re-reduce P_{700}). This means that despite the changes in the energetics of the antenna, the quantum yield of photochemistry of the minimal PSI is the same as in the WT trimeric complex. These results illustrate the functional robustness of this remarkable enzyme.

Nevertheless, we observed differences in the low-temperature fluorescence kinetics of monomeric complexes that parallel the reduction in far-red emission.

Energy equilibration between the bulk antenna and the red Chls in PSI is thought to occur considerably faster than the photochemical trapping, at least at RT, resulting in trapping of a quasiequilibrated state [27,55]. Equilibration times in the order of 3–4 ps have been detected by time-resolved absorption and emission spectroscopy [18,33,34]. Our RT time-resolved fluorescence data are in line with this — although we are not able to resolve lifetimes shorter than ∼10 ps, it is evident that the bulk–red equilibrium is reached well before trapping, which occurs with an effective lifetime of 25 ps. At 77 K, however, the red Chls are populated on different timescales spanning up to 50 ps. ET slows down at lower temperatures, on the one hand because of the reduced spectral overlap and, on the other, because of the restricted uphill transfer. Significant slowdown of ET at 77 K has been shown in different photosynthetic complexes (see [56] and refs. therein, [57]) and also modelled [58,59]. Another possible explanation for the slow spectral changes is that protein dynamics lowers the energy of the red states shifting the emission to longer wavelengths. CT states are associated with large reorganization energies [19,20] and protein motions are generally more temperature-dependent than ET and frozen at cryogenic temperatures [60]. If this is indeed the case, then any assignment of spectral forms to red Chls becomes more difficult as multiple spectral forms originate from CT states involving the same Chl molecules.

Quenching by open and closed RCs

Global analysis of the time-resolved fluorescence data at 77 K resolved three far-red components with lifetimes from ∼200 ps to 1.3 ns (Figure 4), resembling previous results on PSI from *T. elongatus* [38] as well as the PSI core from higher plants [36]. It has been previously postulated that excitations on red Chls can be quenched by the RC (P_{700}) either in its neutral or oxidized (P^+_{700}) state [14,23,38]. The broad near-infrared absorption of P^+_{700} allows it to efficiently quench excitations on the redmost Chls in *Arthrospira* (*Spirulina*) *platensis* and *T. elongatus* [37,38,61]. In the present work, however, we found that P^+_{700} is a less efficient quencher for the red Chls. The different behaviour is probably because of the shorter-wavelength emission of the red Chls in *Synechocystis*, and, consequently, larger spectral overlap with the absorption of P_{700} and smaller overlap with P^+_{700}.

A notable result is that the quenching of red states at 77 K is 30–40% faster in trimers (Figure 5) than in monomers, showing that the oligomeric state of PSI has a measurable effect on the excitation dynamics, at least at low temperature. The differences appear to hold irrespective of the oxidation state of the RC (Table 2). One possible reason for the accelerated fluorescence decay could be connectivity between monomers. Byrdin et al. [37] pointed that the 5 K fluorescence yield of PSI with 50% closed RCs is lower than the expected average yield of PSI with fully open and fully closed RCs, attributing the deviation to inter-monomer transfer. On the other hand, the additional red states in the trimers with intermediate energies between the bulk Chls and the lowest-energy forms, can mediate detrapping of excitations on the latter. As our theoretical calculations indicate, this has a more significant effect on the dynamics.

Theoretical modelling of the excitation dynamics

To aid the interpretation of the results, we created a kinetic model based on the crystal structure of PSI from *Synechocystis* [6], calculating the Förster ET between Chls. The Chl–Chl distances, orientations, and Coulomb couplings are very similar as in Byrdin et al. [23]. To keep the model as simple as possible, we assigned three strongly coupled Chl pairs as the sites of the red states — A32/B7, B31/B32, and B37/B38, carrying a combined oscillator strength equivalent to five Chls. The spectral parameters used for the calculation are shown in Supplementary Table S4. In accordance with the experimental data, the first pair, residing at the monomer–monomer interface, is not the longest-wavelength form but emits at 713 nm in the trimeric PSI. The same three sites have been recently assigned as red Chls in *Synechocystis* PCC 6803 absorbing at 706, 707 and 714 nm [24,62]. We tentatively set the same absorption wavelengths (see Supplementary Table S4), which resulted in an excellent fit of the experimental 77 K absorption and emission spectra (Supplementary Figure S8). We then calculated the Förster ET rates between all Chls in the trimeric and the monomeric complexes. The only change imposed in the monomers was setting the absorption of the pair A32/B7 to 683 nm instead of 706 nm. The simulated DAES (Figure 6) qualitatively resemble the experimental results of both trimers and monomers, mimicking the noteworthy features and differences between them. While it is possible (and probably the case) that additional Chls contribute to the far-red absorption and emission in the real system, the model serves well to illustrate the dynamics of the red Chls and the mechanisms of excitation quenching.

Biochemical Journal (2021) **478** 1333–1346
https://doi.org/10.1042/BCJ20210021

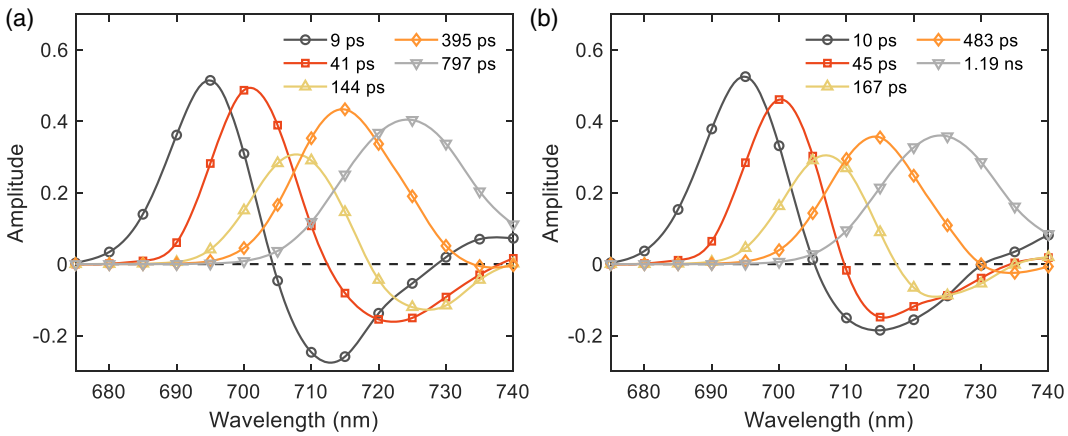

Figure 6. Structure-based simulation of the fluorescence kinetics of PSI.

(**a**) PSI trimers. (**b**) Monomers. The decay-associated emission spectra were obtained by global lifetime analysis of the simulated fluorescence decays.

The model shows ET to red Chls occurring on different timescales and two main decay components in the far-red region, with DAES peaking at 715 and 725 nm. Notably, the final decay lifetimes of the monomers are significantly longer. The model can also reproduce the dependence of the red Chl dynamics on the oxidation state of the RC (Supplementary Table S5). The time-dependent population of the three red Chl states confirms

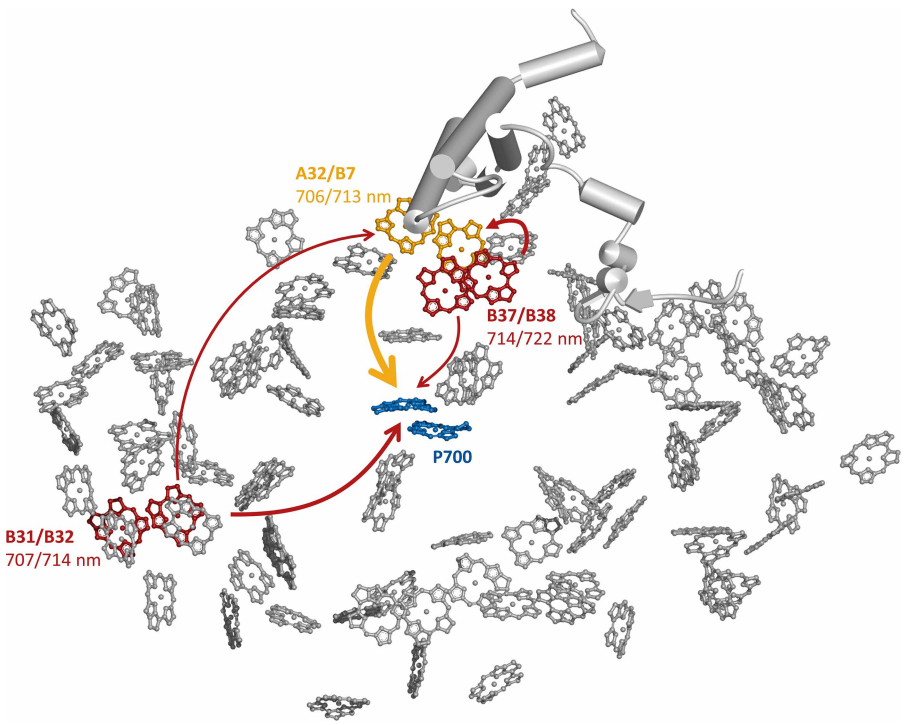

Figure 7. Red Chls in the PSI complex of *Synechocystis* PCC 6803 assigned in the theoretical model based on the crystal structure of trimeric PSI [6] — bulk Chls are in grey, P_{700} in blue, red Chls in yellow/red.

The PsaL subunit is also shown for reference (cylinders). The A32/B7 pair (yellow) harbours a long-wavelength state only in the trimeric complex. The numbers indicate the absorption/emission wavelengths of the red states. The arrows represent different pathways of effective uphill ET from the red Chls to the RC with thicker arrows indicating faster ET.

that B37/B38 is the longest-lived, whereas A32/B7 rapidly decays (Supplementary Figure S9). This is not surprising as the former is the lowest-energy form and A32/B7 is closer and more strongly coupled to P_{700}. In monomers, the decay of the B31/B32 and B37/B38 pairs is slower than in trimers. The main reason for the slowdown is the lack of the red state at A32/B7, which can be verified by comparing the population dynamics in monomers with and without a red state on A32/B7 (Supplementary Figure S10). In other words, the intermediate-energy red state on A32/B7 acts as a bridge between the Chls emitting at longer wavelengths (especially B37/B38) and P_{700}, increasing the overall probability for excitations on the red Chls to be transferred to the RC and used for photochemistry. Obviously, this depends on the mutual arrangement of the red Chls and the RC. The pair A32/B7 located on the donor side of the complex, close to P_{700}, is well positioned to mediate energy transfer from the longest-wavelength form B37/B38 on the stromal side. Figure 7 illustrates the assigned red Chl pairs and the main routes of effective uphill ET between them according to the theoretical calculations. Note that the scheme is only qualitative as the actual ET rates will depend on the exact spectra and transition dipole orientations of the red Chls as well as on whether the RC is open or closed.

Conclusions

In summary, we have resolved the timescales of ET to different red spectral forms in trimeric and monomeric PSI showing that equilibration with the red states spans timescales up to tens of ps competing with photochemical trapping at low temperatures. Excitations are not irreversibly trapped by the red states but are slowly (hundreds of ps) quenched by the RC. Monomeric PSI complexes lacking the PsaL subunit have fewer red Chls emitting at 710–715 nm. The loss of these intermediate-energy Chls results in a slower transfer of excitations from the lowest-energy red Chls (emitting at 720–725 nm) to the RC. Our theoretical calculations support the assignment of the Chl pair A32/B7 as the site of the trimer-specific state and B37/B38 as the site of the lowest-energy state. In PSI trimers, the A32/B7 pair facilitates ET from the lowest-energy state to the RC, thus increasing the overall efficiency of photochemical trapping. Our data also show that, despite a 20% lower protein content, ΔFIJL PSI has virtually identical kinetics of light harvesting and quantum efficiency of charge separation as wild-type PSI under physiological conditions, highlighting the remarkable functional robustness of the PSI core.

Data Availability

The data (absorption spectra, circular dichroism spectra, fluorescence kinetics and DAES) presented in this manuscript are available for download at https://doi.org/10.6084/m9.figshare.13477101.

Competing Interests

The authors declare that there are no competing interests associated with the manuscript.

Funding

The work was supported by grants from the National Research, Development and Innovation Fund, Hungary (NKFI NN-124904, 2018-1.2.1-NKP-2018-00009).

CRediT Contribution

Petar H. Lambrev: Conceptualization, Resources, Software, Supervision, Funding acquisition, Writing — original draft, Project administration, Writing — review and editing. **Parveen Akhtar:** Conceptualization, Resources, Formal analysis, Validation, Investigation, Visualization, Writing — original draft. **Avratanu Biswas:** Resources, Formal analysis, Investigation, Writing — original draft. **László Kovács:** Resources, Formal analysis, Investigation, Writing — review and editing. **Nathan Nelson:** Conceptualization, Writing — review and editing.

Acknowledgements

We are grateful to Prof. Dario Leister and Marcel Dann for providing us the ΔFIJL strain of *Synechocystis*. We thank Terézia Kovács, Éva Herman and Fanny Racskóné Balog-Vig for their technical assistance.

Abbreviations

CD, circular dichroism; CT, charge-transfer; DAES, decay-associated emission spectrum; β-DDM, n-dodecyl β-D-maltoside; ET, energy transfer; PSI, Photosystem I; PSII, Photosystem II; RC, reaction centre; RT, room temperature; TCSPC, time-correlated single-photon counting; WT, wild-type.

Biochemical Journal (2021) **478** 1333–1346
https://doi.org/10.1042/BCJ20210021

References

1 Fromme, P., Jordan, P. and Krauß, N. (2001) Structure of photosystem I. *Biochim. Biophys. Acta* **1507**, 5–31 https://doi.org/10.1016/S0005-2728(01)00195-5

2 Golbeck, J.H. (2003) The binding of cofactors to photosystem I analyzed by spectroscopic and mutagenic methods. *Annu. Rev. Biophys. Biomol. Struct.* **32**, 237–256 https://doi.org/10.1146/annurev.biophys.32.110601.142356

3 Nelson, N. and Junge, W. (2015) Structure and energy transfer in photosystems of oxygenic photosynthesis. *Annu. Rev. Biochem.* **84**, 659–683 https://doi.org/10.1146/annurev-biochem-092914-041942

4 Jordan, P., Fromme, P., Witt, H.T., Klukas, O., Saenger, W. and Krauß, N. (2001) Three-dimensional structure of cyanobacterial photosystem I at 2.5 Å resolution. *Nature* **411**, 909–917 https://doi.org/10.1038/35082000

5 Mazor, Y., Nataf, D., Toporik, H. and Nelson, N. (2014) Crystal structures of virus-like photosystem I complexes from the mesophilic cyanobacterium *Synechocystis* PCC 6803. *eLife* **3**, e01496 https://doi.org/10.7554/eLife.01496

6 Malavath, T., Caspy, I., Netzer-El, S.Y., Klaiman, D. and Nelson, N. (2018) Structure and function of wild-type and subunit-depleted photosystem I in *Synechocystis*. *Biochim. Biophys. Acta* **1859**, 645–654 https://doi.org/10.1016/j.bbabio.2018.02.002

7 Watanabe, M., Kubota, H., Wada, H., Narikawa, R. and Ikeuchi, M. (2011) Novel supercomplex organization of photosystem I in *Anabaena* and *Cyanophora paradoxa*. *Plant Cell Physiol.* **52**, 162–168 https://doi.org/10.1093/pcp/pcq183

8 Ivanov, A.G., Krol, M., Sveshnikov, D., Selstam, E., Sandström, S., Koochek, M. et al. (2006) Iron deficiency in cyanobacteria causes monomerization of photosystem I trimers and reduces the capacity for state transitions and the effective absorption cross section of photosystem I *in vivo*. *Plant Physiol.* **141**, 1436–1445 https://doi.org/10.1104/pp.106.082339

9 Salomon, E. and Keren, N. (2011) Manganese limitation induces changes in the activity and in the organization of photosynthetic complexes in the cyanobacterium *Synechocystis* sp. strain PCC 6803. *Plant Physiol.* **155**, 571–579 https://doi.org/10.1104/pp.110.164269

10 Kłodawska, K., Kovács, L., Várkonyi, Z., Kis, M., Sozer, Ö., Laczkó-Dobos, H. et al. (2015) Elevated growth temperature can enhance photosystem I trimer formation and affects xanthophyll biosynthesis in cyanobacterium *Synechocystis* sp. PCC6803 cells. *Plant Cell Physiol.* **56**, 558–571 https://doi.org/10.1093/pcp/pcu199

11 Netzer-El, S.Y., Caspy, I. and Nelson, N. (2019) Crystal structure of photosystem I monomer from *Synechocystis* PCC 6803. *Front. Plant Sci.* **9**, 1865 https://doi.org/10.3389/fpls.2018.01865

12 Chitnis, V.P. and Chitnis, P.R. (1993) Psal subunit is required for the formation of photosystem I trimers in the cyanobacterium *Synechocystis* sp. PCC 6803. *FEBS Lett.* **336**, 330–334 https://doi.org/10.1016/0014-5793(93)80831-E

13 Xu, Q., Hoppe, D., Chitnis, V.P., Odom, W.R., Guikema, J.A. and Chitnis, P.R. (1995) Mutational analysis of photosystem I polypeptides in the cyanobacterium *Synechocystis* sp. PCC 6803. Targeted inactivation of psaI reveals the function of psaI in the structural organization of psaL. *J. Biol. Chem.* **270**, 16243–16250 https://doi.org/10.1074/jbc.270.27.16243

14 Karapetyan, N.V., Schlodder, E., van Grondelle, R. and Dekker, J.P. (2006) The long-wavelength chlorophylls of photosystem I. In *Photosystem I: The Light-Driven, Plastocyanin:Ferredoxin Oxidoreductase* (Golbeck, J.H., ed.). pp. 177–192, Springer, Dordrecht, The Netherlands

15 Shubin, V., Bezsmertnaya, I. and Karapetyan, N. (1992) Isolation from spirulina membranes of two photosystem I-type complexes, one of which contains chlorophyll responsible for the 77 K fluorescence band at 760 nm. *FEBS Lett.* **309**, 340–342 https://doi.org/10.1016/0014-5793(92)80803-O

16 Vaitekonis, S., Trinkunas, G. and Valkunas, L. (2005) Red chlorophylls in the exciton model of photosystem I. *Photosynth. Res.* **86**, 185–201 https://doi.org/10.1007/s11120-005-2747-x

17 Frese, R.N., Palacios, M.A., Azzizi, A., Van Stokkum, I.H., Kruip, J., Rögner, M. et al. (2002) Electric field effects on red chlorophylls, β-carotenes and P_{700} in cyanobacterial photosystem I complexes. *Biochim. Biophys. Acta* **1554**, 180–191 https://doi.org/10.1016/S0005-2728(02)00242-6

18 Gobets, B. and van Grondelle, R. (2001) Energy transfer and trapping in photosystem I. *Biochim. Biophys. Acta* **1507**, 80–99 https://doi.org/10.1016/S0005-2728(01)00203-1

19 Hayes, J., Matsuzaki, S., Rätsep, M. and Small, G. (2000) Red chlorophyll *a* antenna states of photosystem I of the cyanobacterium *Synechocystis* sp. PCC 6803. *J. Phys. Chem. B* **104**, 5625–5633 https://doi.org/10.1021/jp000447u

20 Rätsep, M., Johnson, T.W., Chitnis, P.R. and Small, G.J. (2000) The red-absorbing chlorophyll *a* antenna states of photosystem I: a hole-burning study of *Synechocystis* sp. PCC 6803 and its mutants. *J. Phys. Chem. B* **104**, 836–847 https://doi.org/10.1021/jp9929418

21 Sener, M.K., Lu, D., Ritz, T., Park, S., Fromme, P. and Schulten, K. (2002) Robustness and optimality of light harvesting in cyanobacterial photosystem I. *J. Phys. Chem. B* **106**, 7948–7960 https://doi.org/10.1021/jp020708v

22 Zazubovich, V., Matsuzaki, S., Johnson, T., Hayes, J., Chitnis, P. and Small, G. (2002) Red antenna states of photosystem I from cyanobacterium *Synechococcus elongatus*: a spectral hole burning study. *Chem. Phys.* **275**, 47–59 https://doi.org/10.1016/S0301-0104(01)00535-3

23 Byrdin, M., Jordan, P., Krauss, N., Fromme, P., Stehlik, D. and Schlodder, E. (2002) Light harvesting in photosystem I: modeling based on the 2.5-Å structure of photosystem I from *Synechococcus elongatus*. *Biophys. J.* **83**, 433–457 https://doi.org/10.1016/S0006-3495(02)75181-3

24 Toporik, H., Khmelnitskiy, A., Dobson, Z., Riddle, R., Williams, D., Lin, S. et al. (2020) The structure of a red-shifted photosystem I reveals a red site in the core antenna. *Nat. Commun.* **11**, 5279 https://doi.org/10.1038/s41467-020-18884-w

25 Hatazaki, S., Sharma, D.K., Hirata, S., Nose, K., Iyoda, T., Kölsch, A. et al. (2018) Identification of short-and long-wavelength emitting chlorophylls in cyanobacterial photosystem I by plasmon-enhanced single-particle spectroscopy at room temperature. *J. Phys. Chem. Lett.* **9**, 6669–6675 https://doi.org/10.1021/acs.jpclett.8b03064

26 Damjanović, A., Vaswani, H.M., Fromme, P. and Fleming, G.R. (2002) Chlorophyll excitations in photosystem I of *Synechococcus elongatus*. *J. Phys. Chem. B* **106**, 10251–10262 https://doi.org/10.1021/jp020963f

27 Croce, R. and van Amerongen, H. (2013) Light-harvesting in photosystem I. *Photosynth. Res.* **116**, 1–14 https://doi.org/10.1007/s11120-013-9838-x

28 Butler, W., Tredwell, C., Malkin, R. and Barber, J. (1979) The relationship between the lifetime and yield of the 735 nm fluorescence of chloroplasts at low temperatures. *Biochim. Biophys. Acta* **545**, 309–315 https://doi.org/10.1016/0005-2728(79)90208-1

29 Jennings, R.C., Zucchelli, G., Croce, R. and Garlaschi, F.M. (2003) The photochemical trapping rate from red spectral states in PSI–LHCI is determined by thermal activation of energy transfer to bulk chlorophylls. *Biochim. Biophys. Acta* **1557**, 91–98 https://doi.org/10.1016/S0005-2728(02)00399-7

30 Searle, G., Barber, J., Harris, L., Porter, G. and Tredwell, C. (1977) Picosecond laser study of fluorescence lifetimes in spinach chloroplast photosystem I and photosystem II preparations. *Biochim. Biophys. Acta* **459**, 390–401 https://doi.org/10.1016/0005-2728(77)90040-8

31 Hastings, G., Kleinherenbrink, F.A., Lin, S. and Blankenship, R.E. (1994) Time-resolved fluorescence and absorption spectroscopy of photosystem I. *Biochemistry* **33**, 3185–3192 https://doi.org/10.1021/bi00177a007
32 Turconi, S., Kruip, J., Schweitzer, G., Rögner, M. and Holzwarth, A.R. (1996) A comparative fluorescence kinetics study of photosystem I monomers and trimers from *Synechocystis* PCC 6803. *Photosynth. Res.* **49**, 263–268 https://doi.org/10.1007/BF00034787
33 Melkozernov, A.N., Lin, S. and Blankenship, R.E. (2000) Excitation dynamics and heterogeneity of energy equilibration in the core antenna of photosystem I from the cyanobacterium *Synechocystis* sp. PCC 6803. *Biochemistry* **39**, 1489–1498 https://doi.org/10.1021/bi991644q
34 Savikhin, S., Xu, W., Chitnis, P.R. and Struve, W.S. (2000) Ultrafast primary processes in PS I from *Synechocystis* sp. PCC 6803: roles of P_{700} and A_0. *Biophys. J.* **79**, 1573–1586 https://doi.org/10.1016/S0006-3495(00)76408-3
35 Melkozernov, A.N., Lin, S., Blankenship, R.E. and Valkunas, L. (2001) Spectral inhomogeneity of photosystem I and its influence on excitation equilibration and trapping in the cyanobacterium *Synechocystis* sp. PCC6803 at 77 K. *Biophys. J.* **81**, 1144–1154 https://doi.org/10.1016/S0006-3495(01)75771-2
36 Akhtar, P. and Lambrev, P.H. (2020) On the spectral properties and excitation dynamics of long-wavelength chlorophylls in higher-plant photosystem I. *Biochim. Biophys. Acta* **1861**, 148274 https://doi.org/10.1016/j.bbabio.2020.148274
37 Byrdin, M., Rimke, I., Schlodder, E., Stehlik, D. and Roelofs, T.A. (2000) Decay kinetics and quantum yields of fluorescence in photosystem I from *Synechococcus elongatus* with P_{700} in the reduced and oxidized state: are the kinetics of excited state decay trap-limited or transfer-limited? *Biophys. J.* **79**, 992–1007 https://doi.org/10.1016/S0006-3495(00)76353-3
38 Shibata, Y., Yamagishi, A., Kawamoto, S., Noji, T. and Itoh, S. (2010) Kinetically distinct three red chlorophylls in photosystem I of *Thermosynechococcus elongatus* revealed by femtosecond time-resolved fluorescence spectroscopy at 15 K. *J. Phys. Chem. B* **114**, 2954–2963 https://doi.org/10.1021/jp909583r
39 Czechowski, N., Lokstein, H., Kowalska, D., Ashraf, K., Cogdell, R. and Mackowski, S. (2014) Large plasmonic fluorescence enhancement of cyanobacterial photosystem I coupled to silver island films. *Appl. Phys. Lett.* **105**, 043701 https://doi.org/10.1063/1.4891856
40 Ciornii, D., Riedel, M., Stieger, K.R., Feifel, S.C., Hejazi, M., Lokstein, H. et al. (2017) Bioelectronic circuit on a 3D electrode architecture: enzymatic catalysis interconnected with photosystem I. *J. Am. Chem. Soc.* **139**, 16478–16481 https://doi.org/10.1021/jacs.7b10161
41 Stieger, K., Feifel, S., Lokstein, H., Hejazi, M., Zouni, A. and Lisdat, F. (2016) Biohybrid architectures for efficient light-to-current conversion based on photosystem I within scalable 3D mesoporous electrodes. *J. Mater. Chem. A* **4**, 17009–17017 https://doi.org/10.1039/C6TA07141D
42 Vajravel, S., Kis, M., Kłodawska, K., Laczko-Dobos, H., Malec, P., Kovács, L. et al. (2017) Zeaxanthin and echinenone modify the structure of photosystem I trimer in *Synechocystis* sp. PCC 6803. *Biochim. Biophys. Acta* **1858**, 510–518 https://doi.org/10.1016/j.bbabio.2017.05.001
43 Zakar, T., Kovacs, L., Vajravel, S., Herman, E., Kis, M., Laczkó-Dobos, H. et al. (2018) Determination of PS I oligomerisation in various cyanobacterial strains and mutants by non-invasive methods. *Photosynthetica* **56**, 294–299 https://doi.org/10.1007/s11099-018-0795-7
44 Lichtenthaler, H.K. (1987) Chlorophylls and carotenoids: pigments of photosynthetic biomembranes. *Methods Enzymol.* **148**, 350–382 https://doi.org/10.1016/0076-6879(87)48036-1
45 Zsiros, O., Ünnep, R., Nagy, G., Almásy, L., Patai, R., Székely, N.K. et al. (2020) Role of protein-water interface in the stacking interactions of granum thylakoid membranes—As revealed by the effects of Hofmeister salts. *Front. Plant Sci.* **11**, 1257 https://doi.org/10.3389/fpls.2020.01257
46 Jeffrey, S., Mantoura, R. and Bjørnland, T. (2005) Data for the identification of 47 key phytoplankton pigments. In *Phytoplankton Pigments in Oceanography: Guidelines to Modern Methods* (Wright, S., Jeffrey, S. and Mantoura, R., eds). pp. 447, UNESCO Publishing, Paris
47 Akhtar, P., Lingvay, M., Kiss, T., Deák, R., Bóta, A., Ughy, B. et al. (2016) Excitation energy transfer between light-harvesting complex II and photosystem I in reconstituted membranes. *Biochim. Biophys. Acta* **1857**, 462–472 https://doi.org/10.1016/j.bbabio.2016.01.016
48 Zakar, T., Herman, E., Vajravel, S., Kovacs, L., Knoppová, J., Komenda, J. et al. (2017) Lipid and carotenoid cooperation-driven adaptation to light and temperature stress in *Synechocystis* sp. PCC6803. *Biochim. Biophys. Acta* **1858**, 337–350 https://doi.org/10.1016/j.bbabio.2017.02.002
49 Gobets, B., van Stokkum, I.H.M., Rogner, M., Kruip, J., Schlodder, E., Karapetyan, N.V. et al. (2001) Time-resolved fluorescence emission measurements of photosystem I particles of various cyanobacteria: a unified compartmental model. *Biophys. J.* **81**, 407–424 https://doi.org/10.1016/S0006-3495(01)75709-8
50 Zsila, F., Molnár, P., Deli, J. and Lockwood, S.F. (2005) Circular dichroism and absorption spectroscopic data reveal binding of the natural cis-carotenoid bixin to human α_1-acid glycoprotein. *Bioorg. Chem.* **33**, 298–309 https://doi.org/10.1016/j.bioorg.2005.03.003
51 Balashov, S.P., Imasheva, E.S. and Lanyi, J.K. (2006) Induced chirality of the light-harvesting carotenoid salinixanthin and its interaction with the retinal of xanthorhodopsin. *Biochemistry* **45**, 10998–11004 https://doi.org/10.1021/bi061098i
52 Chábera, P., Fuciman, M., Hříbek, P. and Polívka, T. (2009) Effect of carotenoid structure on excited-state dynamics of carbonyl carotenoids. *Phys. Chem. Chem. Phys.* **11**, 8795–8803 https://doi.org/10.1039/b909924g
53 Georgakopoulou, S., van Grondelle, R. and van der Zwan, G. (2004) Circular dichroism of carotenoids in bacterial light-harvesting complexes: experiments and modeling. *Biophys. J.* **87**, 3010–3022 https://doi.org/10.1529/biophysj.104.047498
54 Riley, K.J., Reinot, T., Jankowiak, R., Fromme, P. and Zazubovich, V. (2007) Red antenna states of photosystem I from cyanobacteria *Synechocystis* PCC 6803 and *Thermosynechococcus elongatus:* Single-complex spectroscopy and spectral hole-burning study. *J. Phys. Chem. B* **111**, 286–292 https://doi.org/10.1021/jp062664m
55 Melkozernov, A.N. (2001) Excitation energy transfer in Photosystem I from oxygenic organisms. *Photosynth. Res.* **70**, 129–153 https://doi.org/10.1023/A:1017909325669
56 van Grondelle, R., Dekker, J.P., Gillbro, T. and Sundstrom, V. (1994) Energy transfer and trapping in photosynthesis. *Biochim. Biophys. Acta* **1187**, 1–65 https://doi.org/10.1016/0005-2728(94)90166-X
57 Akhtar, P., Do, T.N., Nowakowski, P.J., Huerta-Viga, A., Khyasudeen, M.F., Lambrev, P.H. et al. (2019) Temperature dependence of the energy transfer in LHCII revealed by two-dimensional electronic spectroscopy. *J. Phys. Chem. B.* **123**, 6765–6775 https://doi.org/10.1021/acs.jpcb.9b05421
58 Jia, Y., Jean, J.M., Werst, M.M., Chan, C.-K. and Fleming, G.R. (1992) Simulations of the temperature dependence of energy transfer in the PSI core antenna. *Biophys. J.* **63**, 259–273 https://doi.org/10.1016/S0006-3495(92)81589-8
59 Leng, X., Do, T.N., Akhtar, P., Nguyen, H.L., Lambrev, P. and Tan, H.S. (2020) Hierarchical equations of motion simulation of temperature-dependent two-dimensional electronic spectroscopy of the chlorophyll *a* manifold in LHCII. *Chem. Asian J.* **15**, 1996–2004 https://doi.org/10.1002/asia.202000467

Biochemical Journal (2021) **478** 1333–1346
https://doi.org/10.1042/BCJ20210021

60 Pieper, J., Hauss, T., Buchsteiner, A., Baczyński, K., Adamiak, K., Lechner, R.E. et al. (2007) Temperature- and hydration-dependent protein dynamics in photosystem II of green plants studied by quasielastic neutron scattering. *Biochemistry* **46**, 11398–11409 https://doi.org/10.1021/bi700179s

61 Shubin, V.V., Murthy, S., Karapetyan, N.V. and Mohanty, P. (1991) Origin of the 77 K variable fluorescence at 758 nm in the cyanobacterium *spirulina platensis*. *Biochim. Biophys. Acta* **1060**, 28–36 https://doi.org/10.1016/S0005-2728(05)80115-X

62 Khmelnitskiy, A., Toporik, H., Mazor, Y. and Jankowiak, R. (2020) On the red antenna states of photosystem I mutants from cyanobacteria *synechocystis* PCC 6803. *J. Phys. Chem. B* **124**, 8504–8515 https://doi.org/10.1021/acs.jpcb.0c05201